Heat Mass Transfer (2010) 46:811–819
DOI 10.1007/s00231-010-0644-0

ORIGINAL

Numerical investigation of the influence of incidence angle on asymmetrical turbine blade model showerhead film cooling effectiveness

Mustapha Benabed · Abbès Azzi · B. A. Jubran

Received: 10 October 2008 / Accepted: 9 July 2010 / Published online: 24 July 2010

Abstract The influence of various incidence angles on film cooling effectiveness of an axial turbine blade cascade with leading edge ejection from two rows of cooling holes is numerically investigated. The rows are located in the vicinity of the stagnation line. One row is located on the suction side and the other one is on the pressure side. The predicted pressure field for various blowing ratios ($M = 0.7$, 1.1 and 1.5) is compared with available experimental results at the design condition. Moreover, the effect of various incidence angles ($-10°$, $-5°$, 0°, 5° and 10°) at three blowing rates is investigated by analyzing the results of both laterally averaged and area averaged values of adiabatic film cooling effectiveness. Numerical results indicate that the incidence angle can strongly affect the thermal protection of the blade at low blowing ratio but becomes less dominant at high blowing ratio. In fact, for the low blowing ratio, a small change in the incidence angle that relates to the design condition can deeply affect the thermal protection of the blade, which is evident from the laterally and area averaged film cooling effectiveness distributions.

List of symbols

A	Area, [m^2]
D	Hole diameter, [m]
H	Vane height, [m]
L	Axial chord length, [m]
M	Blowing ratio
Ma	Mach number
Re	Reynolds number
T	Temperature, [K]
Tu	Turbulence intensity, [%]
W	Blade width, [m]
P	Pressure, [Pa]
x, y, z	Cartesian coordinates, [m]
s	Coordinate along vane surface, [m]
t	Pitch, [m]
α, β	Flow angle, [°]
β_S	Staggering angle, [°]
η	Adiabatic film cooling effectiveness
$\bar{\eta}$	Laterally average adiabatic film cooling effectiveness
$\bar{\bar{\eta}}$	Area-averaged effectiveness

Subscripts

aw	Adiabatic wall
c	Cooling air condition
PS	Pressure side
SP	Stagnation point
SS	Suction side

1 Introduction

In order to realize more power and higher thermal efficiency of modern gas turbine, it is essential to increase the turbine inlet temperature (TIT). On average, the TIT is increased continuously by about 20°C a year and can reach about 1,700°C for modern gas turbine. To bypass the limit imposed by the allowable blade metal temperature, it is important to use an advanced cooling method such as the

M. Benabed · A. Azzi
Laboratoire de Mécanique Appliquée,
Faculté de Génie-Mécanique,
Université des Sciences et de la Technologie d'Oran,
B.P. 1505, El-Mnouar, Oran, Algeria

B. A. Jubran (✉)
Department of Aerospace Engineering, Ryerson University,
350 Victoria Street, Toronto, ON, Canada
e-mail: bjubran@ryerson.ca

film cooling. In such situation, the cold air is supplied from the compressor into the turbine blades. The first cooling process is done by convection and then the cold air is ejected through rows of holes into the cascade passage and forms a protection film around the blade. One important design requirement of a film cooling scheme is to reduce the coolant air flow while maintaining minimum aerodynamic losses and high thermal protection. Several theoretical, experimental and numerical investigations have been conducted in order to understand the complex mechanisms of film cooling process. These studies are conducted either for flat plate and/or leading edge turbine blades [1–11] where several geometrical parameters such as the hole length-to-diameter ratio, hole shaped, injection angle and plenum geometry are investigated. Recently, research efforts have been directed toward the development of new injection configurations that help in controlling the coolant flow in the vicinity of the holes [12–15]. The main objective of the above studies is to provide new concepts of geometrical disposition in order to maximize the film cooling effectiveness while retaining the minimum blowing ratio.

Turbulence modeling selection plays an essential role in any numerical investigation such as this presented in this paper. Numerous studies have been conducted on using various turbulence models to predict the thermal and hydrodynamic characteristics of film cooling flow [16–20]. The general consensus is that there is no single turbulence model that is capable of accurately predicting all film cooling flows under different injection configurations, free stream conditions and coolant blowing ratios.

Turbine blades are usually designed to perform at optimum level when the approaching flow is at the right incidence angle design condition. Unfortunately, the mainstream incidence angle on a turbine blade might vary significantly from the design incidence angle due to the unsteady nature of the flow, to changes of the operating conditions or simply to inaccuracies in the predictions of the flow at design conditions. In such situations, the main flow incidence angle is different to that fixed by design conditions and that used in aero thermal investigation. The question now is, how will it be the thermal protection when the main flow is approaching the blade with different incidence angles? To the best of the authors' knowledge, it seems that there is not any conclusive study in the open literature about the effect of incidence angle on film cooling, and this question was firstly posed by Wagner in frame of his Ph.D. thesis at Ecole Polytechnique Federale de Lausanne [21]. His study was conducted experimentally on a blunt body with symmetric leading shape. The aim of the present paper is to shed more light on the effects of the incidence angle on film cooling performance by conducting a numerical investigation using a more realistic gas turbine blade that has been largely documented in the open literature.

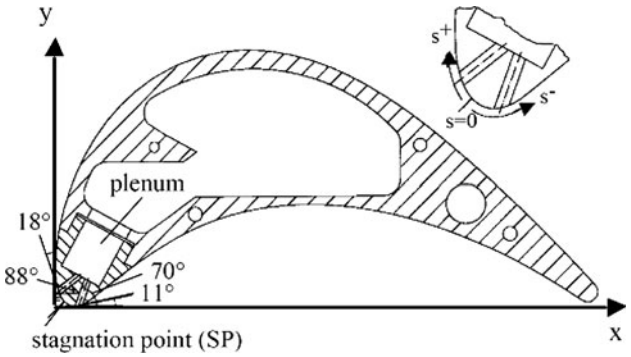

Fig. 1 AGTB B1 blade geometry [24]

Table 1 Cascade geometry and parameters [24]

Geometry	
Chord length (L)	250 mm
Vane height (H)	300 mm
Pitch ratio (t/L)	0.714
Staggering angle (β_S)	73.0°
Aerodynamics	
Inlet Mach number (Ma1)	0.37
Inlet Re number (Re_1)	371,000
Inlet flow angle (α_1)	43°
Isentropic exit Ma number (Ma_{2is})	0.95
Isentropic exit Re number (Re_{2is})	695,000
Exit flow angle (β_2)	28.3°
Cooling configuration (holes)	
Position s/L SS	0.02
Position s/L PS	−0.03
Hole diameter D	3.00 mm
Ejection angle SS	110°
Ejection angle PS	120°
Hole length	12.5 mm

Table 2 Experimental boundary conditions [24]

Flow property			
Blowing ratio	$M = 0.7$	$M = 1.1$	$M = 1.5$
Total pressure $p_{t,1}$	19,620 Pa	19,650 Pa	19,620 Pa
Total temperature $T_{t,1}$	303.15 K	303.15 K	303.15 K
Main flow angle α_1	43°	43°	43°
Static pressure p_2	14,710 Pa	14,640 Pa	14,560 Pa
Cooling fluid inlet conditions			
Total pressure $p_{t,c}$	20,060 Pa	21,710 Pa	24,130 Pa
($T_{t,c}/T_{t,1}$)	1	1	1

Blowing ratio ($M = (\rho c)_c/(\rho c)_1$)

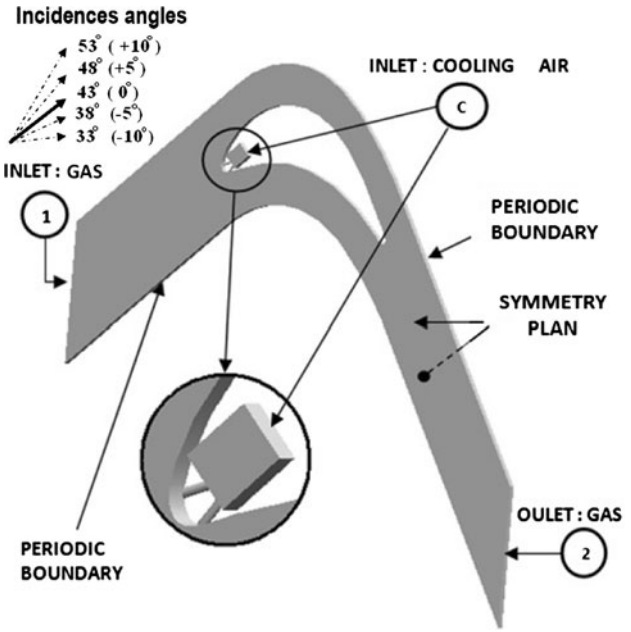

Fig. 2 Flow configuration and boundary conditions

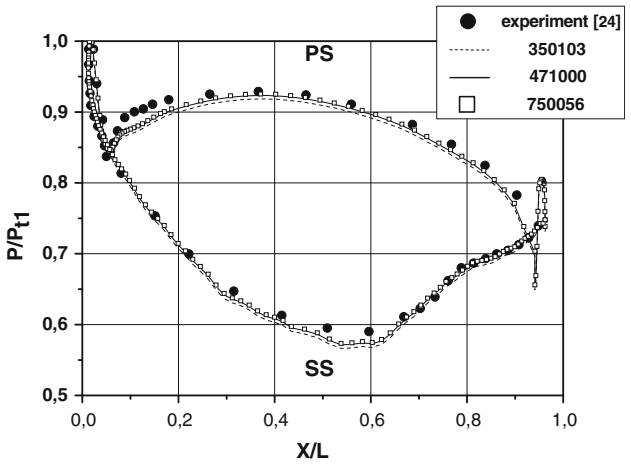

Fig. 3 Grid sensitivity ($M = 0.7$)

2 Presentation of the test case

The blade used here is called the AGTB B1 and corresponds to a high pressure turbine cascade with showerhead injection. The blade is designed with two rows of ejection holes, one in the pressure side (PS) and the other one in the suction side (SS). The two rows are in the vicinity of the leading edge corresponding to a showerhead film cooling configuration (Fig. 1). The experimental studies were conducted in a high speed cascade wind tunnel by Ardey [22–24], who provides the aerodynamic data for several configurations, including streamwise and lateral injections. The choice of range of conditions considered, is according

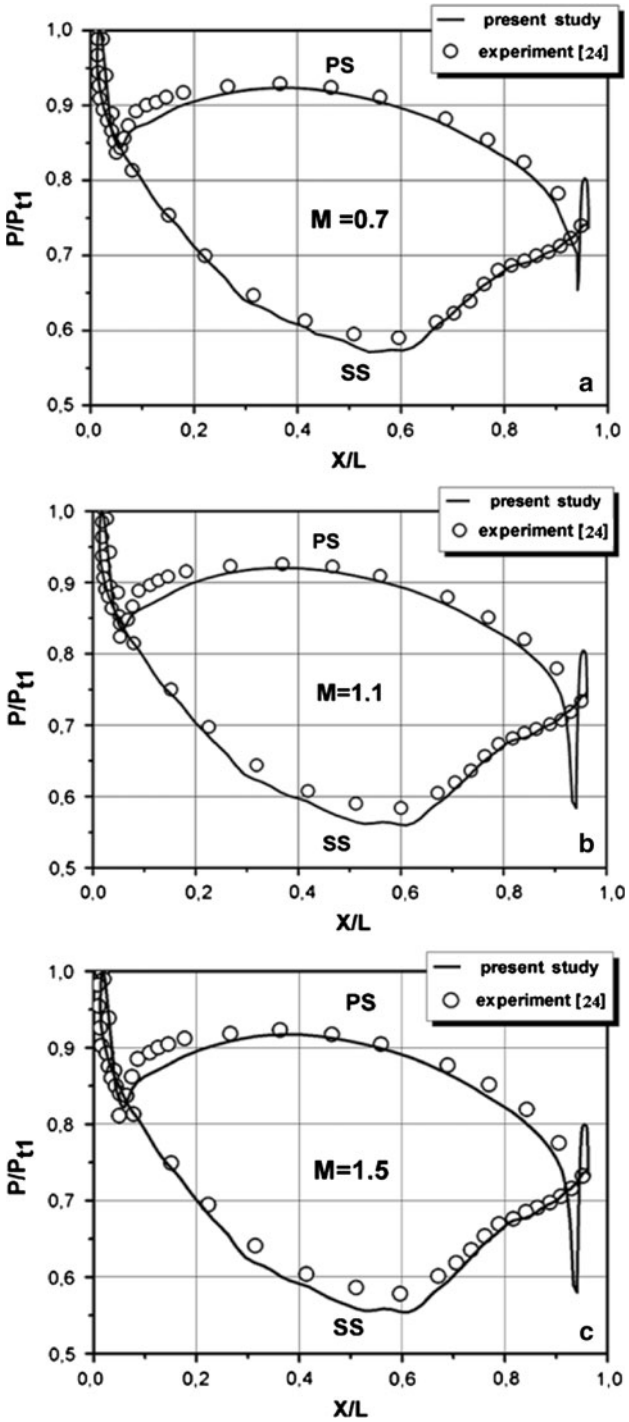

Fig. 4 Static pressure distributions (midplane)

to the capacity of the apparatus used which allows the variation, amongst other things, of Mach number ($0.2 \leq Ma \leq 1.05$) and Reynolds number(10^5 m$^{-1} \leq Re/L \leq 1.5 \times 10^7$ m^{-1}).The geometric data of the cascade can be derived from Table 1. This experimentation has been considered as a test case for the showerhead film cooling configuration by several investigators who have presented

thermal computations that include both streamwise and lateral injections.

The basic case, which corresponds to Ardey's experimentation [24], and which has been used here for computational validation, corresponds to 43° incidence angle to the main flow direction. The boundary conditions used for the basic case are matching those of Ardey and presented on Table 2, which corresponds to three different blowing ratios. Note that in Ardey's experimentation the temperature ratio was maintained to 1, while in the thermal studies [25, 26], the temperature ratio was changed to 0.5 which corresponds to the ratio of the air temperature at the final compressor stage to the turbine inlet temperature under design conditions.

The flow configuration and the boundaries conditions are represented on Fig. 2. The symmetry boundaries are applied at the top and bottom planes bounding the domain. At the two periodic boundaries of the turbine cascade, translational periodicity, with automatic periodic mesh connection method [27], are applied. At the walls, the no-slip condition is used, i.e., the velocity components of the flow are set to zero. The walls are considered as adiabatic boundaries with regard to the energy equation. The fixed static pressure P_2 at the outlet boundary and the total pressure $P_{t,1}$ and the total temperature $T_{t,1}$ at the inlet boundary, are prescribed, such as to match the corresponding experimental conditions (Table 2). Uniform distributions for k and ω were specified, corresponding to a

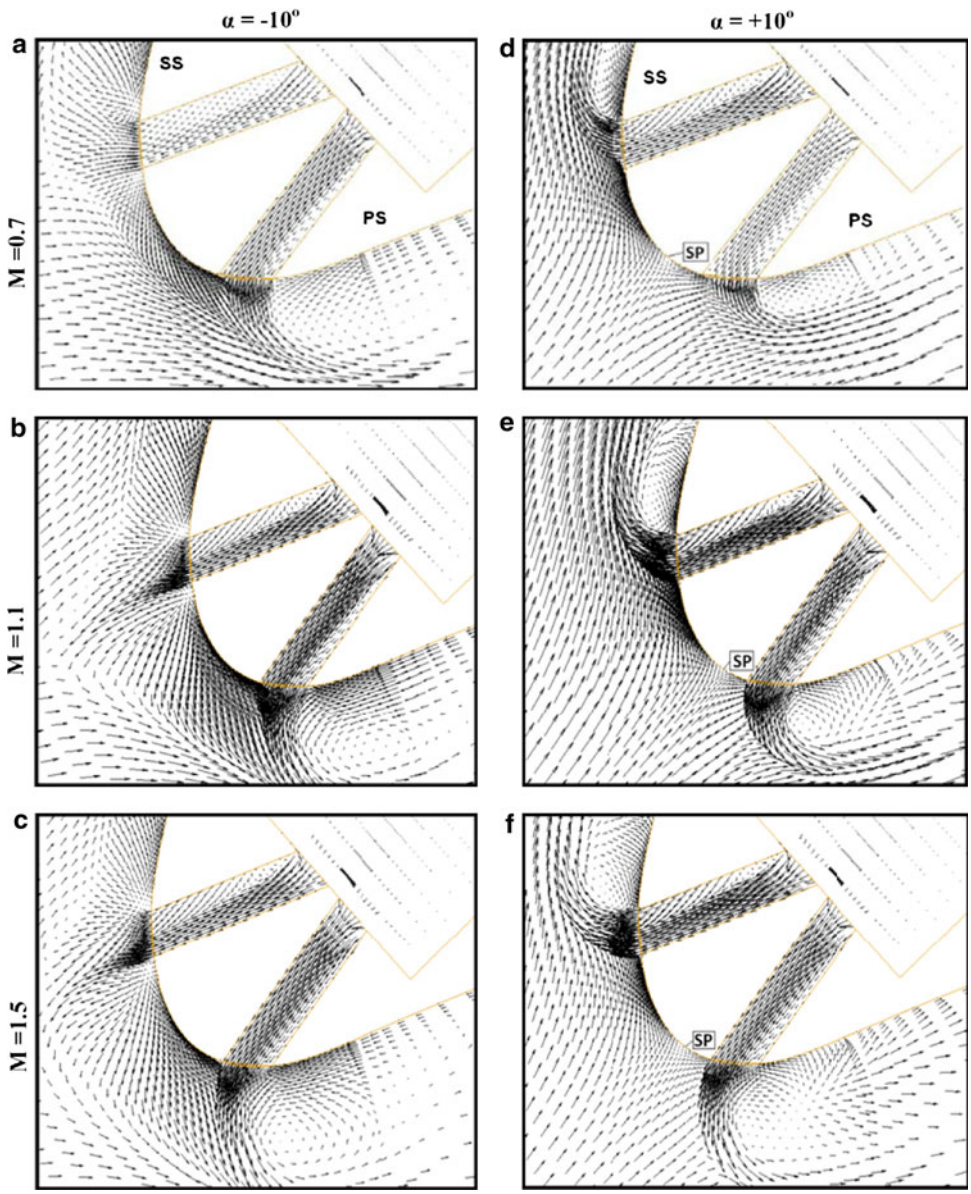

Fig. 5 Leading edge vector plot distributions

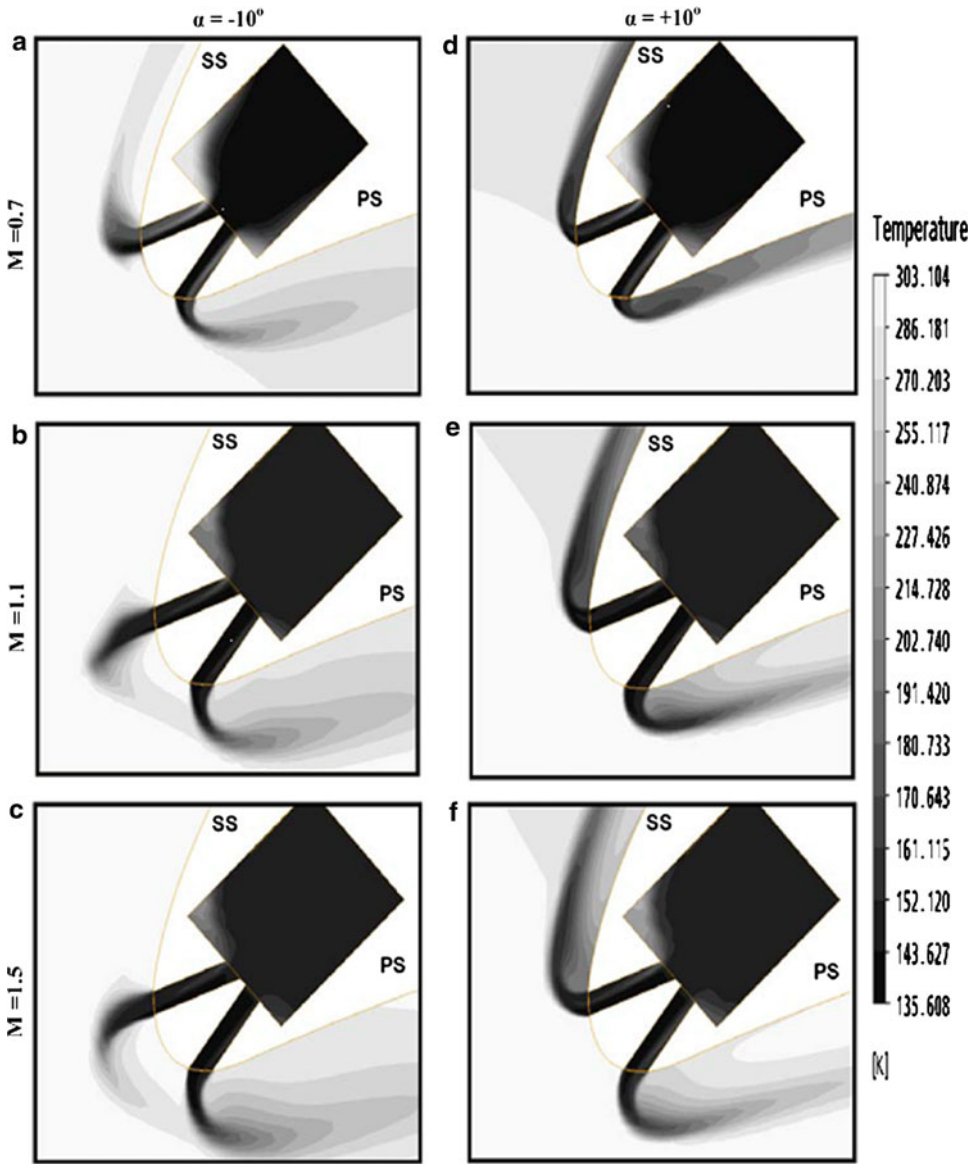

Fig. 6 Computed temperature contours

free-stream turbulence intensity of 5%, and a dimensionless eddy viscosity of 100. In order to simulate the prevailing conditions in the plenum inlet boundary region, lower values are used for both the turbulence intensity and the eddy viscosity (1 and 10%, respectively).

A structured multiblock computational grid was developed using the ICEM grid generator. Three grids of the I type were generated, and referred to as coarse (close to that used by [25]), medium and fine, comprising 350,000, 471,000 and 750,000 hexahedral elements, respectively. Since the computations were performed by the SST model with automatic wall functions [27], care was taken so that the maximum $y+$ at the wall-adjacent cells was kept above the value of 1. A preliminary grid dependence study shows that there are relatively small differences between the three grid results,especially between the medium and fine ones (typically less than 1 percent),as shown in Fig. 3. The medium structured multiblock grid, so, is the best compromise between precision and available computational facilities.

3 Numerical model

The present simulations were conducted using the ANSYS-CFX code [27]. In the solver package, the solution of the Reynolds Averaged Navier-Stokes and energy equations is obtained by using finite volume method with a body-fitted hexahedral structured grid. A co-located layout is employed in which the pressure, turbulence and velocity

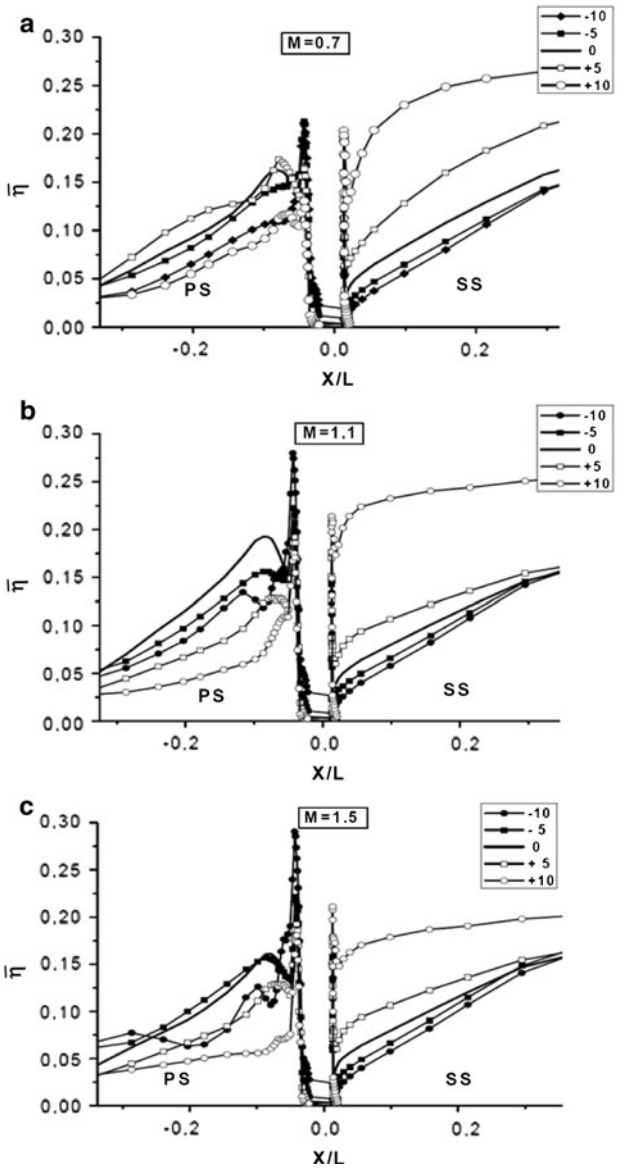

Fig. 7 Laterally averaged film cooling effectiveness at the leading edge

unknowns share the same location. The momentum and continuity equations are coupled through a pressure correction scheme. Several implicit first and second order accurate schemes are implemented for the space and time discretizations. In the present computation, convection terms are discretized with a second order scheme except near discontinuities where it reduces to first order to preserve boundedness.

The turbulence closure is achieved by use of the well known shear stress transport (SST) *k*-omega based model proposed by Menter [28]. This model is known to provide a good compromise by combining the *k*-omega model of Wilcox in the near the wall region and the high Reynolds *k*-eps model in the outer region. The use of the two models is realized via a blending function, which switches from one to zero depending on the geometrical position of the integration point. Detailed explanation of the model formulation and test case validations can be found in specific literature of Menter's group. The turbulent heat flux is modeled by use of the eddy diffusivity hypothesis, where by analogy to eddy viscosity hypothesis, the Reynolds fluxes of a scalar are linearly related to the mean scalar gradient. Eddy diffusivity is related to eddy viscosity by use of a turbulent Prandtl number.

4 Results and discussion

Preliminary computations are done with the same boundary conditions used by Ardey's experimentation. Predicted static pressure distributions for the three blowing ratios along the symmetry plane are compared with the experimental measurements of [24] in Fig. 4. The comparison is satisfactory on the suction side and on the major part of the pressure side. Nevertheless, small differences can be depicted in the front part of the pressure side. In order to investigate the mainstream incidence angle effect on the thermal capability of the blade, four cases are considered in addition to the basic one. For the basic case the mainstream incidence angle is maintained at 43°, while for the other cases it is augmented and reduced by 5 and 10° (Fig. 2). The incidence angle effect is investigated for the three previous blowing ratios, namely $M = 0.7$, 1.1 and 1.5.

Figure 5 shows the vector plot distributions, at the leading edge, for the three blowing ratios and only for the two extreme values of the incidence angle. Globally, the stagnation point moves from the suction side to the pressure side when increasing the incidence angle from $-10°$ (nearly horizontal) up to $+10°$ (nearly vertical). A very interesting effect is observed near the suction side hole injection. In fact, for the lowest blowing ratio and for $-10°$ incidence angle case the stagnation point is close to the suction hole exit. Due to the weak blowing ratio ($M = 0.7$), the cooling jet remains deviated on its predestined side, while for the highest blowing ratios ($M = 1.1$ and 1.5), it is redirected towards the pressure side. This phenomenon is restricted only for $-10°$ mainstream incidence angle. For all cases, increasing blowing ratio results in jet lift off and reverse flow under the jet.

Figure 6 shows temperature contours for the same cases as in Fig. 5. The inversion of the jet deviation cited for $-10°$ and $M = 1.1$ and 1.5 is clearly showed by the thermal contours. Increasing mainstream incidence angle results in a less jet lift off for the suction side hole. The jet is maintained more close to the blade surface and it is expected that film cooling effectiveness increases on the

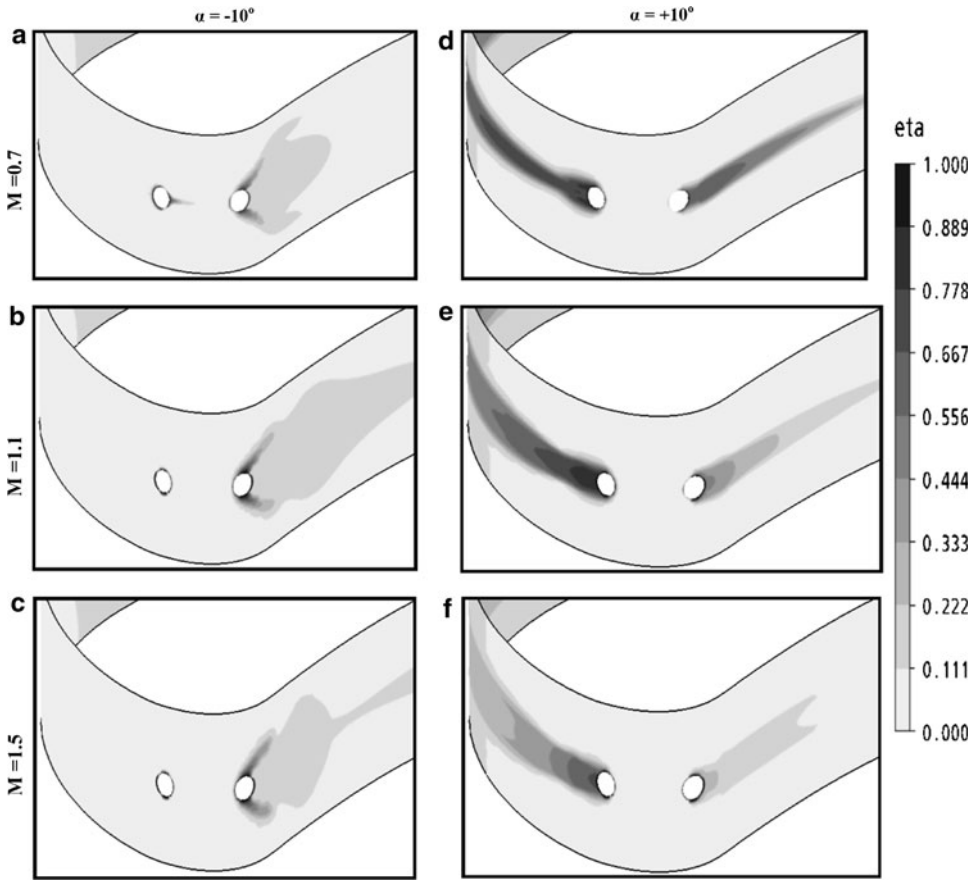

Fig. 8 Leading edge film cooling effectiveness contours

suction side when increasing the mainstream incidence angle.

The analysis of the local adiabatic film cooling effectiveness, the laterally averaged film cooling effectiveness and area-averaged effectiveness is carried out using Eqs. (1), (2), (3), respectively.

$$\eta = \frac{(T_\infty - T_{aw})}{(T_\infty - T_c)} \tag{1}$$

$$\bar{\eta} = \frac{1}{W}\int_0^W \eta(z)dz \tag{2}$$

$$\bar{\bar{\eta}} = \frac{1}{A}\iint \eta dA \tag{3}$$

Figure 7 shows the $\bar{\eta}$ distribution versus the blowing ratio and the incidence mainstream flow angle. For all cases, the zone between the two holes is exposed directly to the hot gases and consequently the effectiveness is in the lowest values. The influence of the incidence mainstream flow angle on the suction side is the same for the three blowing ratios. It increases when the mainstream flow angle incidence increases. However, the situation is more complicated on the pressure side. The tendency for $\bar{\eta}$ is to increase when the mainstream flow angle incidence increases until a specific value, after that the tendency is inversed. The limit value for $M = 0.7$ is $+5°$, for $M = 1.1$ is $0°$ and for $M = 1.5$ is $-5°$.

Figure 8 shows the adiabatic film cooling effectiveness contours on the leading edge at the two extreme incidence angles for $M = 0.7$, 1.1 and 1.5. It is clear from the figure that the hot gas is in direct contact with the blade surface in the stagnation point area between the two holes and hence, a higher thermal load on the blade material is to be expected. In all three cases, the highest effectiveness is occurring near the hole exits and a large region is not covered at all by the cooling air, especially on the suction side. By increasing the incidence angle, from $-10°$ to $+10°$, the adiabatic film cooling effectiveness on the suction side increases notably from the coverage point of view and magnitude, without however detecting a great reduction on the pressure side.

Figure 9 shows the area averaged film cooling effectiveness $\bar{\bar{\eta}}$ on the whole blade surface for various blowing ratios at different incidences angles. Firstly, it is clear that for the negative incidence angles, the increase of the blowing ratio provokes the increase in the area averaged film cooling effectiveness while the opposite happens for the positive incidence angles. However, there is a range of incidence angle $[-3°, -1°]$ where there is just a small

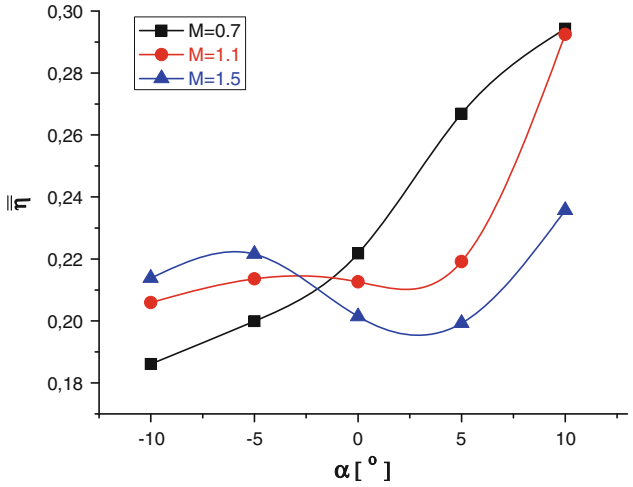

Fig. 9 Area averaged film cooling effectiveness on the blade

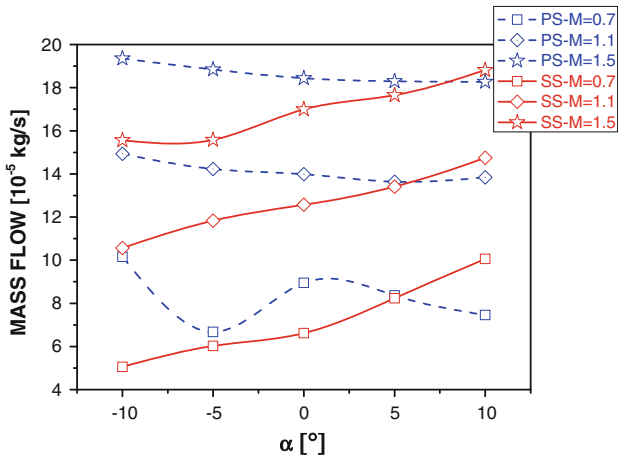

Fig. 10 Cooling mass flow

influence of the blowing ratio. Secondly, for the increase of the incidence angle values from $-10°$ to $+10°$, there is globally an increase in the area averaged film cooling effectiveness, but the increase level is not the same for the three blowing ratios. For $M = 0.7$, $\bar{\bar{\eta}}$ increases monotonically while for $M = 1.1$ and 1.5 the situation is different. For $M = 1.1$ the value is approximately unchanged in the range of $-5°$ to $+5°$ and decreases for $M = 1.5$. This is a very interesting outcome for the combining effect of incidence angle and blowing ratio and need to be investigated in more depth. Figure 10 shows a plot of the cooling injection mass flow from both pressure and suction holes versus the blowing ratios and incidence angles. One important observation is the monotonically increase of the mass flow versus the blowing ratio and incidence angle for the suction side. Nevertheless, for the pressure side the situation is slightly different. The tendency of the mass flow is to decrease when the incidence angle increases except for the lowest blowing ratio ($M = 0.7$).

5 Conclusion

Numerical simulations were performed for film cooling of a leading edge of a turbine blade for various blowing ratios and incidence angles. The primary findings of the present study show that the variation of operating incidence angle from that fixed by design conditions can strongly affect the thermal protection of the blade especially for the low blowing ratios. The stagnation point moves from the suction side to the pressure side when the incidence angle changes from the negative values (nearly horizontal) to the positive ones (nearly vertical). For the lowest value of the incidence angle, the trajectory path of the suction side injection is inversed when the blowing ratio increases, dangerously exposing the suction side to hot gases. Naturally, the thermal protection of the pressure side is increased resulting in a higher globally adiabatic film cooling effectiveness. This can be judged as a good improvement, but the thermal field distribution is highly non uniform and can causes serious damage to the blade. However, increasing the blowing ratio results in a slightly less dramatic change in the thermal field and the influence of incidence angle variation can be small.

References

1. Burd S, Simon T (1997) The influence of coolant supply plenum geometry on coolant exit flow and surface adiabatic effectiveness. ASME paper no. 97-GT-25
2. Lutum E, Johnson B (1999) Influence of the hole length-to-diameter ratio on film cooling with cylindrical holes. ASME J Turbomach 121:209–216
3. Azzi A, Jubran BA (2003) Numerical modeling of film cooling from short length stream-wise injection holes. Heat Mass Transf 39:345–353
4. Bunker RS (2005) A review of Turbine shaped film cooling technology. J Heat Transf 127:441–453
5. Peet YV, Lele SK (2008) Near field of film cooling jet issued into a flat plate boundary layer: LES study. In: Proceedings of ASME Turbo expo 2008. Berlin, Germany, June 9–13
6. Lu Y (2007) Effect of hole configurations on film cooling from cylindrical inclined holes for the application to gas turbine blades. Int J Heat Fluid Flow 28:922–931
7. Mizukami S, Teramoto S, Nagashima T (2007) Numerical study on the three-dimensional flow structure around a film cooling hole. In: Proceedings of international gas Turbine congress 2007(IGTC2007), TS-111
8. Rozati A, Tafti DK (2007) Large eddy simulation of leading edge film cooling part-I: computational domain and effect of coolant inlet condition. ASME Paper No. GT2007-27689, Proceedings ASME Turbo Expo 2007: power for land, sea and air, May 14–17, 2007, Montreal, Canada
9. Azzi A, Jubran BA (2007) Numerical modelling of film cooling from converging slot-hole. J Heat Mass Transf, vol. 43, number 4
10. Baheri S, Alavi Tabrizi SP, Jubran BA (2008) Film cooling effectiveness from trenched shaped and compound holes. J Heat Mass Transf 44(8):989–998

11. Baheri S, Jubran BA, Alavi Tabrizi SP (2008) The effect of turbulence intensity on film cooling of gas turbine blade from trenched shaped holes. ASME paper # GT2008-50318, proceedings of ASME Turbo Expos 2008 conference, June 9–13
12. Javadi A, Javadi K, Taeibi-Rahni M, Darbandi M (2003) A new approach to improve film cooling effectiveness using combined jets. Paper no. IGTC2003Tokyo TS-071
13. Heidmann D (2008) A numerical study of anti-vortex film cooling designs at high blowing ratio. ASME paper no. GT2008-50845
14. Kusterer K, Bohn D, Sugimoto T, Tanaka R (2007) Double-jet ejection of cooling air for improved film cooling. ASME J Turbomach 29:809–815
15. Kusterer K, Bohn D, Sugimoto T (2008) Double-jet film-cooling for highly efficient film-cooling with low blowing ratios. ASME paper no. GT2008-50073
16. Kalita K, Dewan A, Dass A (2002) Prediction of turbulent plane jet in crossflow. Num Heat Transf Part A 41:101–111
17. Ajersch P, Zhou J, Ketler S, Salcudean M, Gartshore I (1997) Multiple jets in a crossflow: detailed measurements and numerical simulations. ASME J Turbomach 119:330–342
18. Harrison K, Bogard D (2008) Comparison of RANS turbulence models for prediction of film cooling performance. ASME paper no. GT2008-51423
19. Nemdili F, Azzi A, Theodoridis G, Jubran BA (2008) Reynolds stress transport modeling of film cooling at the leading edge of a symmetrical turbine blade model. J Heat Transf Eng 29(11): 950–960
20. Baheri S, Alavi Tabrizi SP, Jubran BA (2008) Computational investigation of film cooling from trenched holes near the leading edge of a turbine blade. J Numer Heat Transf Part A Appl 53(3):208–322
21. Wagner G (2007) Experimental investigations of showerhead film cooling on the leading edge of a turbine blade. Ph.D. Thesis no: 3755 (2007), Laboratoire de thermique appliquée et de turbomachines, Ecole Polytechnique Federale de Lausane
22. Ardey S, Fottner L (1997) Flow field measurements on a large scale turbine cascade with leading edge film cooling by two rows of holes. ASME paper no. 97-GT-524
23. Ardey S, Fottner L (1997) A systematic experimental study on the aerodynamics of leading edge film cooling on a large scale high pressure turbine cascade. ASME paper no. 98-GT-434
24. Ardey S (1998) 3D-messung des Strömungsfeldes um die filmgekühlte Vorderkante einer Referenzschaufel. Ph.D. Thesis, University of the Armed Forces Munich
25. Bohn D, Kusterer K (2000) Aerothermal investigation of mixing flow phenomena in case of radially inclined ejection holes at the leading edge. ASME J Turbomach 122:334–339
26. Lakehal D, Theodoridis G, Rodi W (2001) Three dimensional flow and heat transfer calculations of film cooling at the leading edge of asymmetrical turbine blade model. Int J Heat Fluid Flow 22:113–122
27. ANSYS CFX 10.0 (2005) Documentations
28. Menter FR (1993) Zonal two-equation k–ω turbulence model for aerodynamic flows. AIAA paper, 93-2906